



ELSEVIER

Available online at www.sciencedirect.com

SCIENCE @ DIRECT®

Nuclear Physics A 742 (2004) 80–94

NUCLEAR
PHYSICS A

www.elsevier.com/locate/npe

Buda–Lund hydro model for ellipsoidally symmetric fireballs and the elliptic flow at RHIC

M. Csanád^a, T. Csörgő^{b,*}, B. Lörstad^c

^a Department of Atomic Physics, ELTE University, Pázmány P. 1/A, H-1117 Budapest XI, Hungary

^b MTA KFKI RMKI, PO Box 49, H-1525 Budapest 114, Hungary

^c Department of Physics, University of Lund, S-22362 Lund, Sweden

Received 17 October 2003; received in revised form 24 May 2004; accepted 4 June 2004

Available online 14 July 2004

Abstract

The ellipsoidally symmetric extension of Buda–Lund hydrodynamic model is shown here to yield a natural description of the pseudorapidity dependence of the elliptic flow $v_2(\eta)$, as determined recently by the PHOBOS experiment for Au + Au collisions at $\sqrt{s_{NN}} = 130$ and 200 GeV. With the same set of parameters, the Buda–Lund model describes also the transverse momentum dependence of v_2 of identified particles at mid-rapidity. The results confirm the indication for quark deconfinement in Au+Au collisions at RHIC, obtained from a successful Buda–Lund hydro model fit to the single particle spectra and two-particle correlation data, as measured by the BRAHMS, PHOBOS, PHENIX and STAR Collaborations.

© 2004 Elsevier B.V. All rights reserved.

“Nuclei, as heavy as bulls, through collision, generate new states of matter.” (T.D. Lee)

1. Introduction

Ultra-relativistic collisions of almost fully ionized Au atoms are observed in four major experiments at the RHIC accelerator at the highest currently available colliding energies of $\sqrt{s_{NN}} = 200$ GeV to create new forms of matter that existed before in nature only a

* Corresponding author.

E-mail address: csorgo@sunserv.kfki.hu (T. Csörgő).

few microseconds after the big bang, the creation of our Universe. At lower bombarding energies at CERN SPS, collisions of Pb nuclei were studied in the $\sqrt{s_{NN}} = 17$ GeV energy domain, with a similar motivation. If experiments are performed near to the production threshold of a new state of matter, perhaps only the most violent and most central collisions are sufficient to generate a transition to a new state. However, if the energy is well above the production threshold, new states of matter may appear already in the mid-central or even more peripheral collisions. Hence the deviation from axial symmetry of the observed single particle spectra and two-particle correlation functions can be utilized to characterize the properties of such new states.

The PHENIX, PHOBOS and STAR experiments at RHIC produced a wealth of information on the asymmetry of the particle spectra with respect to the reaction plane [1–6], characterized by the second harmonic moment of the transverse momentum distribution, frequently referred to as the “elliptic flow” and denoted by v_2 . This quantity is determined, for various centrality selections, as a function of the transverse mass and particle type at mid-rapidity as well as a function of the pseudo-rapidity $\eta = 0.5 \log\left(\frac{|p|+p_z}{|p|-p_z}\right)$. Pseudorapidity measures the zenithal angle distribution in momentum space, but for particles with high momentum, $|p| \approx E_{|p|}$, it approximates the rapidity $y = 0.5 \log\left(\frac{E+p_z}{E-p_z}\right)$ that characterizes the longitudinal momentum distribution and transforms additively for longitudinal boosts, hence the rapidity density dn/dy is invariant for longitudinal boosts. The PHOBOS Collaboration found [3], that $v_2(\eta)$ is a strongly decreasing function of $|\eta|$, which implies that the concept of boost-invariance, suggested by Bjorken in Ref. [7] to characterize the physics of very high energy heavy ion collisions, cannot be applied to characterize the hadronic final state of Au + Au collisions at RHIC. A similar conclusion can be drawn from the measurement of the inhomogeneous (pseudo)rapidity $dn/d\eta$ and dn/dy distributions of charged particle production at RHIC by both the BRAHMS [8] and PHOBOS [9] Collaborations, proving the lack of boost-invariance in these reactions, as $dn/dy \neq \text{const}$ at RHIC. Although many models describe successfully the transverse momentum dependence of the elliptic flow at mid-rapidity, $v_2(p_t, \eta = 0)$, see Refs. [10,11] for recent reviews on this topic, to our best knowledge and an up-to-date scanning of the available high energy and nuclear physics literature, no model has yet been able to reproduce the measured pseudo-rapidity dependence of the elliptic flow at RHIC.

Hence we present here the first successful attempt to describe the pseudo-rapidity dependence of the elliptic flow $v_2(\eta)$ at RHIC. Our tool is the Buda–Lund hydrodynamic model [12,13], which we extend here from axial to ellipsoidal symmetry. The Buda–Lund hydro model takes into account the finite longitudinal extension of the particle emitting source, and we show here how the finite longitudinal size of the source leads naturally to a v_2 that decreases with increasing values of $|\eta|$, in agreement with the data. We describe simultaneously the pseudorapidity and the transverse momentum dependence of the elliptic flow, with a parameter set, that reproduces the single-particle transverse momentum and pseudo-rapidity distributions as well as the radius parameters of the two-particle Bose–Einstein correlation functions, or HBT radii, in case when the orientation of the event plane is averaged over. All these benefits are achieved with the help of transparent and simple analytic formulas, that are natural extensions of our earlier results to the case of ellipsoidal symmetry.

2. Buda–Lund hydro for ellipsoidal expansions

The Buda–Lund model is defined with the help of its emission function $S(x, p)$, where $x = (t, r_x, r_y, r_z)$ is a point in space–time and $p = (E, p_x, p_y, p_z)$ stands for the four-momentum. To take into account the effects of long-lived resonances, we utilize the core–halo model [14], and characterize the system with a hydrodynamically evolving core and a halo of the decay products of the long-lived resonances. Within the core–halo picture, the measured intercept parameter λ_* of the two-particle Bose–Einstein correlation function is related [14] to the strength of the relative contribution of the core to the total particle production at a given four-momentum

$$S(x, p) = S_c(x, p) + S_h(x, p), \quad (1)$$

$$S_c(x, p) = \sqrt{\lambda_*} S(x, p). \quad (2)$$

Based on the success of the Buda–Lund hydro model to describe Au + Au collisions at RHIC [15,26], Pb + Pb collisions at CERN SPS [16] and $h + p$ reactions at CERN SPS [17, 18], we assume that the core evolves in a hydrodynamical manner

$$S_c(x, p) d^4x = \frac{g}{(2\pi)^3} \frac{p^\mu d^4 \Sigma_\mu(x)}{B(x, p) + s_q}, \quad (3)$$

where g is the degeneracy factor ($g = 1$ for identified pseudoscalar mesons, $g = 2$ for identified spin = 1/2 baryons), and $p^\mu d^4 \Sigma_\mu(x)$ is a generalized Cooper–Frye term, describing the flux of particles through a distribution of layers of freeze-out hypersurfaces, $B(x, p)$ is the (inverse) Boltzmann phase-space distribution, and the term s_q is determined by quantum statistics, $s_q = 0, -1$, and $+1$ for Boltzmann, Bose–Einstein and Fermi–Dirac distributions, respectively.

For a hydrodynamically expanding system, the (inverse) Boltzmann phase-space distribution is

$$B(x, p) = \exp\left(\frac{p^\nu u_\nu(x)}{T(x)} - \frac{\mu(x)}{T(x)}\right). \quad (4)$$

We will utilize some ansatz for the shape of the flow four-velocity, $u_\nu(x)$, chemical potential, $\mu(x)$, and temperature, $T(x)$ distributions. Their form is determined with the help of recently found exact solutions of hydrodynamics, both in the relativistic [19–21] and in the non-relativistic cases [22–24], with the conditions that these distributions are characterized by mean values and variances, and that they lead to (simple) analytic formulas when evaluating particle spectra and two-particle correlations.

The generalized Cooper–Frye prefactor is determined from the assumption that the freeze-out happens, with probability $H(\tau) d\tau$, at a hypersurface characterized by $\tau = \text{const}$ and that the proper-time measures the time elapsed in a fluid element that moves together with the fluid, $d\tau = u^\mu(x) dx_\mu$. We parameterize this hypersurface with the coordinates (r_x, r_y, r_z) and find that $d^3 \Sigma^\mu(x|\tau) = u^\mu(x) d^3x/u^0(x)$. Using $\partial_\tau \tau|_r = u^0(x)$ we find that in this case the generalized Cooper–Frye prefactor is

$$p^\mu d^4 \Sigma_\mu(x) = p^\mu u_\mu(x) H(\tau) d^4x. \quad (5)$$

This finding generalizes the result of Ref. [25] from the case of a spherically symmetric Hubble flow to anisotropic, direction dependent Hubble flow distributions.

From the analysis of CERN SPS and RHIC data [15,16,26], we find that the proper-time distribution in heavy ion collisions is rather narrow, and $H(\tau)$ can be well approximated with a Gaussian representation of the Dirac-delta distribution

$$H(\tau) = \frac{1}{(2\pi\Delta\tau^2)^{1/2}} \exp\left(-\frac{(\tau - \tau_0)^2}{2\Delta\tau^2}\right), \quad (6)$$

with $\Delta\tau \ll \tau_0$.

Based on the success of the Buda–Lund hydro model to describe the axially symmetric collisions, we develop an ellipsoidally symmetric extension of the Buda–Lund model, that goes back to the successful axially symmetric case [12,13,15,16,26] if axial symmetry is restored, corresponding to the $X = Y$ and $\dot{X} = \dot{Y}$ limit of the model described below.

We specify a fully scale invariant, relativistic form, which reproduces known non-relativistic hydrodynamic solutions too, in the limit when the expansion is non-relativistic. Both in the relativistic and the non-relativistic cases, the ellipsoidally symmetric, self-similarly expanding hydrodynamical solutions can be formulated in a simple manner, using a scaling variable s and a corresponding four-velocity distribution u^μ , that satisfy

$$u^\mu \partial_\mu s = 0, \quad (7)$$

which means that s is a good scaling variable if its co-moving derivative vanishes [19, 20]. This equation couples the scaling variable s and the flow velocity distribution. It is convenient to introduce the dimensionless, generalized space–time rapidity variables (η_x, η_y, η_z) , defined by the identification of

$$(\sinh \eta_x, \sinh \eta_y, \sinh \eta_z) = \left(r_x \frac{\dot{X}}{X}, r_y \frac{\dot{Y}}{Y}, r_z \frac{\dot{Z}}{Z} \right). \quad (8)$$

Here (X, Y, Z) are the characteristic sizes (for example, the lengths of the major axis) of the expanding ellipsoid, that depend on proper-time τ and their derivatives with respect to proper-time are denoted by $(\dot{X}, \dot{Y}, \dot{Z})$. The distributions will be given in this η_i variables, but the integral-form is the standard $d^4x = dt dr_x dr_y dr_z$, so we have to take a Jacobi-determinant into account. Eq. (7) is satisfied by the choice of

$$s = \frac{\cosh \eta_x - 1}{\dot{X}_f^2} + \frac{\cosh \eta_y - 1}{\dot{Y}_f^2} + \frac{\cosh \eta_z - 1}{\dot{Z}_f^2}, \quad (9)$$

$$u^\mu = (\gamma, \sinh \eta_x, \sinh \eta_y, \sinh \eta_z), \quad (10)$$

and from here on $(\dot{X}_f, \dot{Y}_f, \dot{Z}_f) = (\dot{X}(\tau_0), \dot{Y}(\tau_0), \dot{Z}(\tau_0)) = (\dot{X}_1, \dot{X}_2, \dot{X}_3)$, assuming that the rate of expansion is constant in the narrow proper-time interval of the freeze-out process. The above form has the desired non-relativistic limit

$$s \rightarrow \frac{r_x^2}{2X_f^2} + \frac{r_y^2}{2Y_f^2} + \frac{r_z^2}{2Z_f^2}, \quad (11)$$

where again $(X_f, Y_f, Z_f) = (X(\tau_0), Y(\tau_0), Z(\tau_0)) = (X_1, X_2, X_3)$. From now on, we drop subscript f . From the normalization condition of $u^\mu(x)u_\mu(x) = 1$ we obtain that

$$\gamma = \sqrt{1 + \sinh^2 \eta_x + \sinh^2 \eta_y + \sinh^2 \eta_z}. \quad (12)$$

For the fugacity distribution we assume a shape, that leads to Gaussian profile in the non-relativistic limit

$$\frac{\mu(x)}{T(x)} = \frac{\mu_0}{T_0} - s, \quad (13)$$

corresponding to the solution discussed in Refs. [22,23,27]. We assume that the temperature may depend on the position as well as on proper-time. We characterize the inverse temperature distribution similarly to the shape used in the axially symmetric model of Refs. [12,13], and discussed in the exact hydro solutions of Refs. [22,23]

$$\frac{1}{T(x)} = \frac{1}{T_0} \left(1 + \frac{T_0 - T_s}{T_s} s \right) \left(1 + \frac{T_0 - T_e}{T_e} \frac{(\tau - \tau_0)^2}{2\Delta\tau^2} \right) \quad (14)$$

where T_0 , T_s and T_e are the temperatures of the center, and the surface at the mean freeze-out time τ_0 , while T_e corresponds to the temperature of the center after most of the particle emission is over (cooling due to evaporation and expansion). Sudden emission corresponds to $T_e = T_0$, and the $\Delta\tau \rightarrow 0$ limit. It is convenient to introduce the following quantities:

$$a^2 = \frac{T_0 - T_s}{T_s} = \left\langle \frac{\Delta T}{T} \right\rangle_r, \quad (15)$$

$$d^2 = \frac{T_0 - T_e}{T_e} = \left\langle \frac{\Delta T}{T} \right\rangle_t. \quad (16)$$

In the above approach we assume the validity of the concept of local thermalization and the concept of ellipsoidal symmetry at the time of particle production. We do not know, what freeze-out condition is realized exactly in Nature. Our above formulas can be also considered as a general, second order Taylor expansion of the inverse temperature and logarithmic fugacity distributions, which maintains ellipsoidal symmetry. We attempt to determine the coefficients of this Taylor expansion from the data in the subsequent parts. As the saddle-point calculation presented below is sensitive only to second order Taylor coefficients, any model that has similar second order expansion leads to similar results. A more theoretical approach is to solve relativistic hydrodynamics for ellipsoidally expanding fireballs and to apply the presently most advanced freeze-out criteria, for example the method of escaping probabilities developed by Akkelin, Hama and Sinyukov in Ref. [28].

We also note that the applied distribution of freeze-out temperatures goes back to the dynamical calculation of Ref. [29]. This calculation starts from an initial condition at $\tau = 3.5$ fm/c, which was given by a parton cascade model (PCM) calculation for Au + Au collisions at $\sqrt{s_{NN}} = 200$ GeV. This initial condition is followed by a three-dimensional Hubble flow. In addition, this dynamical calculation determined the thermodynamical constraints of entropy and local energy–momentum conservation for a sudden time-like deflagration from a supercooled quark–gluon plasma (QGP) phase to a pion gas phase. Such a transition may start at a constant proper-time, at some (position independent) value of the local temperature, that corresponds to the supercooled quark–gluon plasma (QGP) phase. Such sudden hadronization from a supercooled QGP phase can be realized due to the large characteristic nucleation times of hadronic bubbles inside a supercooled QGP, see Ref. [29] for details. The strong three-dimensional expansion leads to negative pressures, mechanical instabilities and the resulting timelike deflagration may produce hadronic final

states in the hatched area of Fig. 1 of Ref. [29]. Half of this area corresponds to superheated hadron gas, with *hadronic* temperatures in the range of 1.0–1.4 T_c , while half of available final states are hadron gas states below the critical temperature, with hadronic temperatures of 0.8–1.0 T_c . Thus it is reasonable to assume, that in a realistic situation, the hadronic final states correspond to a range of temperatures even if the transition starts from the same temperature everywhere on a constant proper-time hypersurface. The variation can only be increased if the temperature of the prehadronic state happened to be inhomogeneous on a constant proper-time hypersurface. This is why we have assumed in the present paper, that the hadronic temperatures may be position dependent on a constant proper-time hypersurface. Instead of using a priori assumptions, we determine the parameter values of the hadronic local temperature distribution a posteriori, from recent data on Au + Au collisions at RHIC.

3. Integration and saddlepoint approximation

The observables are calculated analytically from the Buda–Lund hydro model, using a saddle-point approximation in the integration. This approximation is exact both in the Gaussian and the non-relativistic limit, and if $p^\nu u_\nu/T \gg 1$ at the point of maximal emissivity. In this approximation, the emission function looks like

$$S(x, k) d^4x = \frac{g}{(2\pi)^3} \frac{p^\mu u_\mu(x_s) H(\tau_s)}{B(x_s, p) + s_q} \exp(-R_{\mu\nu}^{-2} (x - x_s)^\mu (x - x_s)^\nu) d^4x, \quad (17)$$

where

$$R_{\mu\nu}^{-2} = \partial_\mu \partial_\nu (-\ln(S_0))_s, \quad (18)$$

and x_ν stands here for (τ, r_x, r_y, r_z) . In the integration, a Jacobian τ/t has to be introduced when changing the integration measure from d^4x to $d\tau d^3x$.

The position of the saddle-point can be calculated from the equation

$$\partial_\mu (-\ln(S_0))(x_s, p) = 0. \quad (19)$$

Here we introduced S_0 , as the “narrow” part of the emission function:

$$S_0(x, p) = \frac{H(\tau)}{B(x, p) + s_q}. \quad (20)$$

In general, we get the following for the saddle-point in $(\tau, \eta_x, \eta_y, \eta_z)$ coordinates:

$$\tau_s = \tau_0, \quad (21)$$

$$\sinh \eta_{i,s} = \frac{p_i \dot{X}_i^2 \cosh \eta_{i,s}}{T(x_s) \left(1 + a^2 \frac{p_\mu u^\mu(x_s)}{T_0}\right) + p_0 \frac{\cosh \eta_{i,s}}{\gamma(x_s)} \dot{X}_i^2}. \quad (22)$$

The system of equations (22) can be solved efficiently for the saddle-point positions $\eta_{s,i}$ using a successive approximation. This method was implemented in our data analysis. For the widths of the distributions, we obtained exact analytic results, given in terms of $\eta_{s,i}$ that we determined from the successive approximations. We have used the full expressions,

obtained simply with the help of derivations at the saddle-point, for the evaluation of the observables and for the comparison with the data. However, we summarize here only the leading order approximative result, due to reasons of clarity and transparency.

In the simplest case, where all three $\eta_{i,s}$ are small:

$$\frac{r_{i,s}}{X_i} = \frac{\frac{p_i}{T_0} \dot{X}_i}{1 + \frac{X_i^2}{R_{T,i}^2}}, \quad \text{for } i = x, y, z, \quad (23)$$

$$\frac{1}{R_{i,i}^2} = \frac{B(x_s, p)}{B(x_s, p) + s_q} \left(\frac{1}{X_i^2} + \frac{1}{R_{T,i}^2} \right), \quad (24)$$

$$\frac{1}{R_{0,0}^2} = \frac{1}{\Delta\tau_*^2} = \frac{1}{\Delta\tau^2} + \frac{B(x_s, p)}{B(x_s, p) + s} \frac{1}{\Delta\tau_T^2}. \quad (25)$$

Eqs. (24), (25) imply, that the HBT radii are dominated by the smaller of the thermal and the geometrical length scales in all directions, as found in Refs. [12,13]. Note that the geometrical scales stem from the density distribution, governed by the fugacity term $\exp[\mu(x)/T(x)]$, while the thermal lengths originate from the local thermal momentum distribution $\exp[-p^\mu u_\mu(x)/T(x)]$, and in the above limit they are

$$\frac{1}{\Delta\tau_T^2} = \frac{m_T}{T_0} \frac{d^2}{\tau_0^2}, \quad (26)$$

$$\frac{1}{R_{T,i}^2} = \frac{m_T}{T_0} \left(\frac{a^2}{X_i^2} + \frac{\dot{X}_i^2}{X_i^2} \right). \quad (27)$$

4. The invariant momentum distribution

The invariant momentum distribution can be calculated as

$$N_1(p) = \int d^4x S(x, p) = \frac{1}{\sqrt{\lambda_*}} \int d^4x S_c(p, x). \quad (28)$$

The result is a simple expression:

$$N_1(p) = \frac{g}{(2\pi)^3} \bar{E} \bar{V} \bar{C} \frac{1}{\exp\left(\frac{p^\mu u_\mu(x_s) - \mu(x_s)}{T(x_s)}\right) + s_q}, \quad (29)$$

where

$$\bar{E} = p_\mu u^\mu(x_s), \quad (30)$$

$$\bar{V} = (2\pi)^{3/2} \frac{\Delta\tau_*}{\Delta\tau} [\det R_{ij}^2]^{1/2}, \quad (31)$$

$$\bar{C} = \frac{1}{\sqrt{\lambda_*}} \frac{\tau_s}{t_s}. \quad (32)$$

Let us investigate the structure of this invariant momentum distribution, in particular, the exponent of the spectrum. Let us introduce

$$b(x_s, p) = \log B(x_s, p), \quad (33)$$

and evaluate this exponent in the limit, where the saddle-point coordinates are all small,

$$b(x_s, p) = \frac{p_x^2}{2\bar{m}_t T_{*,x}} + \frac{p_y^2}{2\bar{m}_t T_{*,y}} + \frac{p_z^2}{2\bar{m}_t T_{*,z}} + \frac{\bar{m}_t}{T_0} - \frac{p_t^2}{2\bar{m}_t T_0} - \frac{\mu_0}{T_0}, \quad (34)$$

where the direction dependent slope parameters are

$$T_{*,x} = T_0 + \bar{m}_t \dot{X}^2 \frac{T_0}{T_0 + \bar{m}_t a^2}, \quad (35)$$

$$T_{*,y} = T_0 + \bar{m}_t \dot{Y}^2 \frac{T_0}{T_0 + \bar{m}_t a^2}, \quad (36)$$

$$T_{*,z} = T_0 + \bar{m}_t \dot{Z}^2 \frac{T_0}{T_0 + \bar{m}_t a^2}, \quad (37)$$

and

$$\bar{m}_t = m_t \cosh(\eta_{z,s} - y). \quad (38)$$

In the limit when we neglect the possibility of a temperature inhomogeneity on the freeze-out hypersurface, $a = 0$, and using a non-relativistic approximation of $\bar{m}_t \approx m$, we recover the recent result of Ref. [27] for the mass dependence of the slope parameters of the single-particle spectra:

$$T_{*,x} = T_0 + m \dot{X}^2, \quad (39)$$

$$T_{*,y} = T_0 + m \dot{Y}^2, \quad (40)$$

$$T_{*,z} = T_0 + m \dot{Z}^2. \quad (41)$$

5. The elliptic flow

Note, that $b(x_s, p)$ is the only part of the IMD, that is explicitly angle dependent, so

$$\begin{aligned} N_1(p) &\sim \exp\left(-\frac{p_x^2}{2\bar{m}_t T_{*,x}} - \frac{p_y^2}{2\bar{m}_t T_{*,y}}\right) \\ &= \exp\left(-\frac{p_t^2}{2\bar{m}_t T_{\text{eff}}} + \left(\frac{p_t^2}{2\bar{m}_t T_{*,x}} - \frac{p_t^2}{2\bar{m}_t T_{*,y}}\right) \frac{\cos(2\varphi)}{2}\right), \end{aligned} \quad (42)$$

where

$$T_{\text{eff}} = \frac{1}{2} \left(\frac{1}{T_{*,x}} + \frac{1}{T_{*,y}} \right). \quad (43)$$

So, we can easily extract the angular dependencies. Let us compute v_2 by integrating on the angle:

$$v_2 = \frac{I_1(w)}{I_0(w)}, \quad (44)$$

where

$$w = \frac{p_t^2}{4\bar{m}_t} \left(\frac{1}{T_{*,y}} - \frac{1}{T_{*,x}} \right). \quad (45)$$

Generally, we get from the definition

$$N_1 = \frac{d^3n}{dp_z p_t dp_t d\varphi} = \frac{d^2n}{2\pi dp_z p_t dp_t} \left[1 + 2 \sum_{n=1}^{\infty} v_n \cos(n\varphi) \right] \quad (46)$$

the following equations:

$$v_{2n} = \frac{I_n(w)}{I_0(w)}, \quad (47)$$

$$v_{2n+1} = 0. \quad (48)$$

As first and the third flow coefficients vanish in this case, a tilt angle ϑ has to be introduced to get results compatible with observations, as discussed in the subsequent parts.

For large rapidities, $|\eta_s - y|$ becomes also large, and $\bar{m}_t = m_t \cosh(\eta_s - y)$ diverges, hence $w \rightarrow 0$. Thus we find a natural mechanism for the decrease of v_2 for increasing values of $|y|$, as in this limit, $v_2 \rightarrow I_1(0)/I_0(0) = 0$.

6. Elliptic flow for tilted ellipsoidal expansion

Now, let us compute the elliptic flow for tilted, ellipsoidally expanding sources, too, because we can get a non-vanishing v_1 and v_3 only this way, in case of $\vartheta \neq 0$, similarly to the non-relativistic case discussed in Ref. [27]. The observables are determined in the center of mass frame of the collision (CMS), where the r_x axis points to the direction of the impact parameter and the r_z axis points to the direction of the beam. In this frame, the ellipsoidally expanding fireball, described in the previous sections, may be rotated. So let us assume, that we relabel all the x and p coordinates in the previous parts with the superscript $'$, e.g., $x \rightarrow x'$ and $p \rightarrow p'$, to indicate that these calculations were performed in the system of ellipsoidal expansion (SEE), where the principal axis of the expanding ellipsoid coincide with the principal axis of SEE. In the following, we use the unprimed variables to denote quantities defined in the CMS, the frame of observation.

We assume, that the initial conditions of the hydrodynamic evolution correspond to a rotated ellipsoid in CMS [27]. The tilt angle ϑ represents the rotation of the major (longitudinal) direction of expansion, r'_z , from the direction of the beam, r_z . Hence the event plane is the (r'_x, r'_z) plane, which is the same, as the (r_x, r_z) plane. The (zenithal) angle between directions r_z and r'_z is the tilt angle ϑ , while (azimuthal) angle φ is between the event plane and the direction of the transverse momentum p_t .

From the invariant momentum distribution, v_m can be calculated as follows:

$$v_m = \int_0^{2\pi} \frac{\frac{dn}{dp_z p_t dp_t d\varphi}}{\frac{dn}{dp_z p_t dp_t 2\pi}} \cos(m\varphi) d\varphi. \quad (49)$$

We have made the coordinate transformation

$$p'_x = p_x \cos \vartheta - p_z \sin \vartheta, \quad (50)$$

$$p'_y = p_y, \quad (51)$$

$$p'_z = p_z \cos \vartheta + p_x \sin \vartheta, \quad (52)$$

and in addition:

$$p_x = p_t \cos \varphi, \quad (53)$$

$$p_y = p_t \sin \varphi, \quad (54)$$

and calculated the transverse momentum and the pseudorapidity dependence of v_2 , for a parameter set determined from fitting the axially symmetric version of the Buda–Lund hydro model to single particle pseudo-rapidity distribution of BRAHMS [8] and PHOBOS [9], the mid-rapidity transverse momentum spectra of identified particles as measured by PHENIX [30,31] and the two-particle Bose–Einstein correlation functions or HBT radii as measured by the PHENIX [32] and STAR [33] Collaborations.

We determined the harmonic moment of Eq. (49) numerically, for the case of $m = 2$, but using the analytic expression of Eq. (29) for the invariant momentum distribution, computing the coordinates of the saddle point with a successive approximation. The successive approximation means a loop here instead of solving the non-analytic saddle-point equations. We have chosen a loop long enough and have checked that an even longer loop will not modify the results. This was the same with the width of the integration-step. We integrated $N_1(p)$ over p_t , as the data were taken this way, too. Finally, we were able to describe $v_2(\eta = 0, p_t)$ and $v_2(\eta)$ with the same set of parameters.

The results are summarized both in Figs. 1 and 2. We find that a small asymmetry in the expansion gives a natural description of the transverse momentum dependence of v_2 . The parameters are taken from the previous Buda–Lund hydro model fits to the two-particle Bose–Einstein correlation data (HBT radii) and the single particle spectra of Au + Au collisions at $\sqrt{s_{NN}} = 130$ GeV, Refs. [15,26], where the axially symmetric version of the model was utilized. Here we have introduced parameters that control the asymmetry of the expansion in the X and Y directions such a way that the angular averaged, effective source is unchanged. For example, we required that the effective temperature, T_{eff} of Eq. (43) is unchanged. We see on Figs. 1 and 2 that this method was successful in reproducing the data on elliptic flow, with a small asymmetry between the two transverse expansion rates.

The identified particle elliptic flow measurement of PHENIX used a method of determining the reaction plane from the particles at large rapidities, hence its results are not significantly affected by non-flow correlations, see Ref. [1]. Fig. 1. illustrates the quality of agreement between our Buda–Lund model calculation and this PHENIX data set. From the parameter values corresponding to Fig. 1, we calculate the value of the $v_2(\eta = 0)$ and find that this value is below the published PHOBOS data point at mid-rapidity by 0.02. Note, that in order to compute $v_2(\eta)$, one has to integrate $N_1(\eta, p_t, \phi)$ over p_t first, and determine the elliptic flow from the p_t integrated, η and ϕ dependent spectra, as the PHOBOS

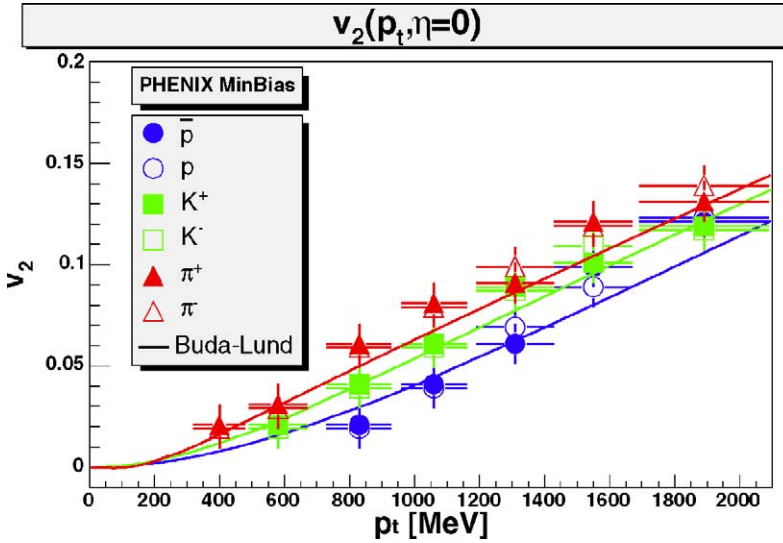


Fig. 1. Buda–Lund model calculation and the $v_2(p_t, \eta = 0)$ data. Ellipsoidally symmetric Buda–Lund calculation compared to the PHENIX $v_2(p_t)$ data of identified particles [1]. The parameter set is: $T_0 = 210$ MeV, $\dot{X} = 0.57$, $\dot{Y} = 0.45$, $\dot{Z} = 2.4$, $a = 1$, $\tau_0 = 7$ fm/c, $\vartheta = 0.09$, $X_f = 8.6$ fm, $Y_f = 10.5$ fm, $Z_f = 17.5$ fm, $\mu_{0,\pi} = 70$ MeV, $\mu_{0,K} = 210$ MeV and $\mu_{0,p} = 315$ MeV, and the masses are taken as their physical value.

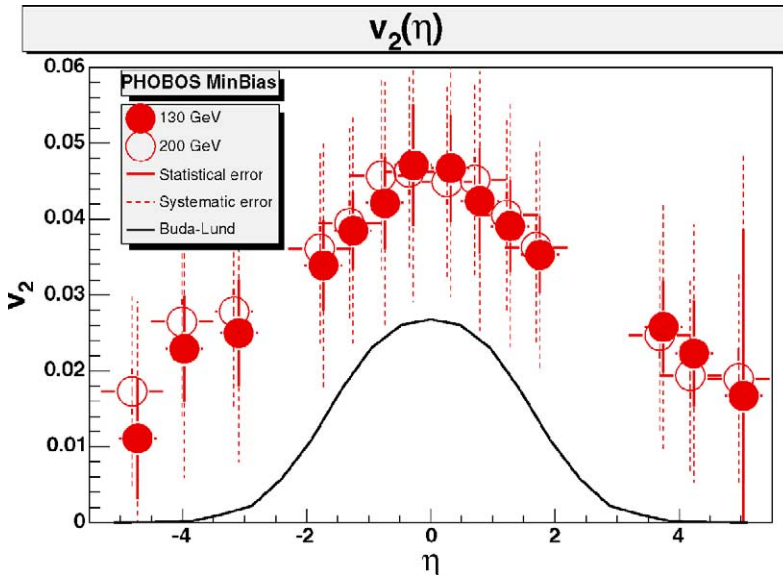


Fig. 2. Buda–Lund model calculation and the $v_2(\eta)$ data. This image compares the ellipsoidally symmetric Buda–Lund model to the 130 GeV Au + Au and 200 GeV Au + Au $v_2(\eta)$ data of PHOBOS [3,4]. Here we used the same parameter set as in Fig. 1, with pion mass and chemical potential, and indicated a systematic error, corresponding to a non-flow parameter of 0.01, on the PHOBOS data. The parameters of the Buda–Lund model are determined here from other observables, they will be optimized to $v_2(\eta)$ data in a subsequent publication.

Table 1

The table shows the parameter set used to describe the data. Note, that $a^2 = (T_0 - T_s)/T_s$, see Eq. (15)

Parameter	Value
T_0	210 MeV
\dot{X}	0.57
\dot{Y}	0.45
\dot{Z}	2.4
a	1
τ_0	7 fm/c
$\Delta\tau$	0 fm/c
ϑ	0.09
X_f	8.6 fm
Y_f	10.5 fm
Z_f	17.5 fm
$\mu_{0,\pi}$	70 MeV
$\mu_{0,K}$	210 MeV
$\mu_{0,p}$	315 MeV

data were taken this way, too. Because of this, there is no simple mathematical connection between $v_2(p_t, \eta = 0)$, and $v_2(\eta)$ as they do not stem from a common $v_2(p_t, \eta)$ function.

The PHOBOS Collaboration pointed out the possible existence of a non-flow contribution in their v_2 data, see Ref. [3], as they did not utilize the fourth order cumulant method to determine v_2 . We attribute the 0.02 difference between the present Buda–Lund model calculation and the PHOBOS data point at mid-rapidity to such a non-flow contribution [34]. The magnitude of the non-flow contribution has been explicitly studied (but in a different acceptance, at mid-rapidity) by the STAR Collaboration. STAR found that its value is of the order of 0.01 for mid-rapidity minimum bias data in the STAR acceptance, Ref. [5].

The good description of the $dn/d\eta$ distribution by the Buda–Lund hydro model [15,26] is well reflected in the good description of shape of the pseudo-rapidity dependence of the elliptic flow. Thus the finiteness of the expanding fireball in the longitudinal direction and the scaling three-dimensional expansion is found to be responsible for the experimentally observed violations of the boost invariance of both the rapidity distribution and that of the collective flow v_2 .

Table 1 summarizes the parameter values corresponding to Figs. 1 and 2. These indicate a high, $T_0 > T_c = 170$ MeV central temperature, with a cold surface temperature of $T_s \approx 105$ MeV. The success of this description suggests that a small fraction of pions may be escaping from the fireball from a superheated hadron gas, which can be considered as an indication, that part of the source of Au + Au collisions at RHIC may be a deconfined matter with $T > T_c$.

Let us determine the size of the volume that is above the critical temperature. Within this picture, one can find the critical value of $s = s_c$ from the relation that $T_0/(1 + as_c) = T_c$. Using $T_0 = 210$ MeV, $T_c = 170$ MeV, and $a = 1$ we find $s_c = 0.235$. The surface of the ellipsoid with $T \geq T_c$ is given by

$$\frac{r_x^2}{X_c^2} + \frac{r_y^2}{Y_c^2} + \frac{r_z^2}{Z_c^2} = 1. \quad (55)$$

The principal axes of the “critical” ellipsoid are given by $X_c = X_f \sqrt{s_c} \simeq 4.2$ fm, $Y_c = Y_f \sqrt{s_c} \simeq 5.1$ fm, $Z_c = Z_f \sqrt{s_c} \simeq 8.5$ fm, hence the volume of the ellipsoid with $T > T_c$ is $V_c = \frac{4\pi}{3} X_c Y_c Z_c \approx 753$ fm³.

Note, however, that the characteristic average or surface temperature of the fireball within this model is $T_s = T_0/(1+a) \approx 105$ MeV. So the picture is similar to a snow-ball which has a melted core inside.

Our study shows that this picture is consistent with the pseudorapidity and transverse mass dependence of v_2 at RHIC in the soft $p_t < 2$ GeV domain, however, it is not yet a direct proof of the existence of a new phase. Among others, we have to determine precisely the errors on the best fit parameters and to determine the confidence levels of the fits, which will be a subject of further research.

In discussing the significance of the results, it is useful to compare it to other calculations to find similarities and differences as well as to map out directions for possible further research. For us the key point is not the good agreement between the model and the data, but the analytic insight and the functional relationships between the model parameters and the observables. We checked the model against the data only to demonstrate that we are on a good track to understand the rapidity dependence of the elliptic and higher order flows, but the fine-tuning of the model parameters is a subject of further investigations.

It seems, that our most important result are Eqs. (38), (45), (47), (48), that explain analytically why all higher order flows vanish at very forward or backward rapidities. Due to the finite longitudinal size of the source, the point of maximal emittivity moves to the summit of the expanding ellipsoid as the rapidity is increased to high values. Due to the Hubble flow, the transverse momentum distribution has negligible transverse flow contributions at this point, the local temperature plays the dominant role. However, the local temperature contributes equally in both transverse directions, hence all second and higher order flows vanish at very forward rapidities. Similar observations hold in the very backward direction, due to symmetry reasons.

When comparing to earlier calculations, we observe that the two key features, the finite longitudinal size and the three-dimensional Hubble flow were not present simultaneously in other works as far as we know. Also, the temperature variations, the cooling on the surface were not considered by other attempts to understand elliptic flow. For example, Hirano and Tsuda considered a three-dimensional numerical solution of relativistic hydrodynamics in Ref. [35]. Their model is not too far from the considerations presented here, they have a finite longitudinal extension of the source and a well developed transverse flow at mid-rapidity. Their Fig. 9 indicates that they obtained a vanishing elliptic flow at very forward and backward rapidities. However, they utilized a Bjorken type initial condition, and the concept of a constant freeze-out temperature. As a result, their elliptic flow is approximately rapidity independent near mid-rapidity, which is not surprising, given the boost invariant initial condition for the flow velocity distribution. Hirano studied in Ref. [36] the effects of short lived resonance decays on the rapidity dependence of the elliptic flow at SPS energies. His result is that resonance decays yield a negative non-flow contribution, ranging from -0.15 at mid-rapidity to about -0.05 at forward and backward rapidities. We did not explore the consequences of such an effect here, however, its magnitude is about the size of the error bars on the PHOBOS data. This is one of the interesting directions that can be explored in further studies, and the importance of this effect will increase at RHIC

as more and more high statistics, precision measurements will be available on the elliptic flow.

7. Summary and conclusions

We have generalized the Buda–Lund hydro model to the case of ellipsoidally symmetric expanding fireballs. As we derived simple formulas for the rapidity and transverse momentum dependence of the elliptic flow, we gave qualitative as well as analytic insight to the rapidity dependence of the elliptic flow.

When comparing to data, we kept the parameters determined from earlier fits to the single particle spectra and the two-particle Bose–Einstein correlation functions (HBT radii) [15,26], and interpreted them as angular averages for the direction of the reaction plane. Then we found that a small splitting between the expansion rates parallel and transverse to the direction of the impact parameter, as well as a small zenithal tilt of the particle emitting source is sufficient to describe simultaneously the transverse momentum dependence of the elliptic flow of identified particles [1] at mid-rapidity in Au + Au collisions at $\sqrt{s_{NN}} = 200$ GeV. Already with this simple method, we describe qualitatively the pseudo-rapidity dependence of the collective flow as measured in Refs. [3,4], taking into account an overall 0.01 systematic error on these data points, as estimated in Ref. [5]. As Fig. 2 indicates, for the given parameter set the Buda–Lund model systematically under-estimates the pseudo-rapidity dependent elliptic flow, within 2–3 standard deviations at each point, but the shape is well reproduced. The best fit parameters to $v_2(p_t, \eta)$ will be determined from an automatized fit parameter optimization in a subsequent publication.

The results support the indication for quark deconfinement at RHIC found in Refs. [15,26], based on the observation, that some of the particles are emitted from a region with higher than the critical temperature, $T > T_c = 170$ MeV. We estimated that the size of this volume is about (1/8)th of the total volume measured on the $\tau = \tau_0$ main freeze-out hypersurface, totaling of about 753 fm^3 . However, the analysis indicates that the average or surface temperature is rather cold, $T_s \approx 105$ MeV, so approximately 7/8 of the particles are emitted from a rather cold hadron gas.

Acknowledgements

T.Cs. would like to thank B. Lörstad and G. Gustafson for kind hospitality during his stay at the University of Lund in spring 2003. The support of the following grants are gratefully acknowledged: OTKA T038406, T034269, the exchange programmes of the OTKA, MTA and NSF under grant INT0089462 and the Hungarian and Polish Academy of Sciences, as well as the NATO PST.CLG grant 980086.

References

- [1] PHENIX Collaboration, S.S. Adler, et al., Phys. Rev. Lett. 91 (2003) 182301, nucl-ex/0305013.
- [2] PHENIX Collaboration, K. Adcox, et al., Phys. Rev. Lett. 89 (2002) 212301, nucl-ex/0204005.
- [3] PHOBOS Collaboration, B.B. Back, et al., Phys. Rev. Lett. 89 (2002) 222301, nucl-ex/0205021.

- [4] PHOBOS Collaboration, S. Manly, et al., Nucl. Phys. A 715 (2003) 611, nucl-ex/0210036.
- [5] STAR Collaboration, C. Adler, et al., Phys. Rev. C 66 (2002) 034904, nucl-ex/0206001.
- [6] STAR Collaboration, C. Adler, et al., Phys. Rev. Lett. 87 (2001) 182301, nucl-ex/0107003.
- [7] J.D. Bjorken, Phys. Rev. D 27 (1983) 140.
- [8] BRAHMS Collaboration, I.G. Bearden, et al., Phys. Rev. Lett. 90 (2003) 102301.
- [9] PHOBOS Collaboration, B.B. Back, et al., Phys. Rev. Lett. 87 (2001) 102303, nucl-ex/0106006.
- [10] W. Reisdorf, H.G. Ritter, Annu. Rev. Nucl. Part. Sci. 47 (1997) 663.
- [11] S.A. Voloshin, Nucl. Phys. A 715 (2003) 379, nucl-ex/0210014.
- [12] T. Csörgő, B. Lörstad, Phys. Rev. C 54 (1996) 1390, hep-ph/9509213.
- [13] T. Csörgő, B. Lörstad, Nucl. Phys. A 590 (1995) 465c, hep-ph/9503494.
- [14] T. Csörgő, B. Lörstad, J. Zimányi, Z. Phys. C 71 (1996) 491, hep-ph/9411307.
- [15] T. Csörgő, A. Ster, Heavy Ion Phys. 17 (2003) 295, nucl-th/0207016.
- [16] A. Ster, T. Csörgő, B. Lörstad, Nucl. Phys. A 661 (1999) 419, hep-ph/9907338.
- [17] EHS/NA22 Collaboration, N.M. Agababian, et al., Phys. Lett. B 422 (1998) 359, hep-ex/9711009.
- [18] T. Csörgő, Heavy Ion Phys. 15 (2002) 1, hep-ph/0001233.
- [19] T. Csörgő, F. Grassi, Y. Hama, T. Kodama, Phys. Lett. B 565 (2003) 107, nucl-th/0305059.
- [20] T. Csörgő, L.P. Csernai, Y. Hama, T. Kodama, Acta Phys. Hungar. A: Heavy Ion Phys. 21 (2004) 73–84, nucl-th/0306004.
- [21] T. Csörgő, Y. Hama, in preparation.
- [22] T. Csörgő, nucl-th/9809011, Centr. Eur. J. Phys. (2004), in press.
- [23] T. Csörgő, hep-ph/0111139.
- [24] T. Csörgő, J. Zimányi, Heavy Ion Phys. 17 (2003) 281, nucl-th/0206051.
- [25] W. Florkowski, W. Florkowski, Phys. Rev. Lett. 87 (2001) 272302, nucl-th/0106050;
W. Florkowski, W. Florkowski, Nucl. Phys. A 715 (2003) 875, nucl-th/0208061;
W. Florkowski, W. Florkowski, AIP Conf. Proc. 660 (2003) 177, nucl-th/0212052;
W. Florkowski, A. Baran, W. Florkowski, AIP Conf. Proc. 660 (2003) 185, nucl-th/0212053.
- [26] M. Csanád, T. Csörgő, B. Lörstad, A. Ster, in: Proc. Int. Symp. Multipart. Dyn. (2003), Acta Phys. Pol. B 35 (2004) 191–196, <http://th-www.if.uj.edu.pl/ismd2003/Talks/Ster.ppt>.
- [27] T. Csörgő, S.V. Akkelin, Y. Hama, B. Lukács, Y.M. Sinyukov, Phys. Rev. C 67 (2003) 034904, hep-ph/0108067.
- [28] Y.M. Sinyukov, S.V. Akkelin, Y. Hama, Phys. Rev. Lett. 89 (2002) 052301, nucl-th/0201015.
- [29] T. Csörgő, L.P. Csernai, Phys. Lett. B 333 (1994) 494, hep-ph/9406365.
- [30] PHENIX Collaboration, K. Adcox, et al., Phys. Rev. C 69 (2004) 024904, nucl-ex/0307010.
- [31] PHENIX Collaboration, S.S. Adler, et al., Phys. Rev. C 69 (2004) 034909, nucl-ex/0307022.
- [32] PHENIX Collaboration, K. Adcox, et al., Phys. Rev. Lett. 88 (2002) 192302, nucl-ex/0201008.
- [33] STAR Collaboration, C. Adler, et al., Phys. Rev. Lett. 87 (2001) 082301, nucl-ex/0107008.
- [34] N. Borghini, P.M. Dinh, J.Y. Ollitrault, Phys. Rev. C 63 (2001) 054906, nucl-th/0007063;
N. Borghini, P.M. Dinh, J.Y. Ollitrault, Phys. Rev. C 64 (2001) 054901, nucl-th/0105040.
- [35] T. Hirano, K. Tsuda, Phys. Rev. C 66 (2002) 054905, nucl-th/0205043.
- [36] T. Hirano, Phys. Rev. Lett. 86 (2001) 2754, nucl-th/0004029.